Letters

Optimized Kilowatt-Range Boost Converter Based on Impulse Rectification With 52 kW/l and 98.6% Efficiency

Armin Jafari, *Student Member, IEEE*, Mohammad Samizadeh Nikoo, *Member, IEEE*, Remco van Erp, and Elison Matioli, *Member, IEEE*

***Abstract*—Maximizing the efficiency and power density of dc–dc converters demands parallel optimizations in design and control, especially for variable-frequency converters operating over wide frequency ranges. This letter presents the full-scale optimization of a kilowatt-range megahertz-class boost converter based on the impulse rectification. To maximize the heat extraction from the converter and increase its power density, the entire power stage is implemented on a single-layer insulated-metal substrate. For high efficiencies over wide frequency ranges, high-performance gallium nitride transistors are employed and various high-frequency materials (MnZn, NiZn, and air) with different geometries are compared to realize a wide-bandwidth inductor. Silicon carbide Schottky diodes with a zero reverse recovery are utilized for efficient high-frequency rectification, and the impact of the device's current rating on its generated reactive power and the overall system efficiency are investigated at different power levels up to 1 kW. The proposed optimum duty cycle control maximizes the conversion efficiency at different gains and powers and prevents fatal device hard switching at high frequencies. The optimized converter enables a peak efficiency of 98.6% along with an ultrahigh power density of 52 kW/l (850 W/in^3). A loss breakdown summarizes major efficiency bottlenecks to be overcome by future advances in power electronics.**

***Index Terms*—Boost, dc–dc, gallium nitride (GaN), high-frequency, high power density, impulse rectification, insulated-metal substrate printed circuit board (IMS PCB), optimum duty cycle control, silicon carbide (SiC), soft-switching, wide-bandwidth inductor.**

I. Introduction

HIGH-PERFORMANCE gallium nitride (GaN) and silicon carbide (SiC) devices enable soft-switched converters to operate efficiently at high frequencies [1]; nonetheless, simultaneous maximization of efficiency and power density, typically two opposing objectives, requires an advanced hardware configuration—from the printed circuit board (PCB) design for an efficient heat extraction to the high-quality passive component design and proper wide-band-gap device selection—as well as optimum control strategies [2].

Boost converters are the main building blocks in power electronics and are used in a wide range of applications. In a conventional boost converter, the transistor is subjected to hard switching, which hinders its efficient operation at very high frequencies and in turn results in higher inductor volumes. A boost converter based on the impulse rectification can potentially overcome the aforementioned drawbacks by maintaining soft switching [3]. This letter focuses on a full-scale hardware and control optimization of a boost converter based on the impulse rectification, resulting in a kilowatt-range megahertz-class converter design with an outstanding power density of 52 kW/l (850 W/in^3) and a peak efficiency of 98.6%. First, we demonstrate the PCB design on a single-layer insulated-metal substrate (IMS) that enabled an ultrahigh power density. Next, the high-frequency magnetic materials with different winding geometries are compared to realize a wide-bandwidth inductor. A discussion on the diode selection is followed by introducing an optimum duty cycle control method for maximizing the efficiency over the entire voltage gains and power levels. A loss breakdown is presented to identify the efficiency bottleneck, and the concurrently superior efficiency and power density of the boost converter are benchmarked against the state-of-the-art dc–dc converters.

II. Design for Ultrahigh Density

The main challenges for realizing an ultrahigh density converter are the efficient thermal interface design and reduced high-frequency losses [4]. To obtain an efficient thermal interface, the entire power stage was implemented on a single-layer IMS PCB, as shown in Fig. 1(a). The IMS technology is known for its outstanding thermal performance in high-power light-emitting diodes and high-speed motor drives [5], [6]. Fig. 1(b) presents the full converter design, including the high-frequency inductor along with the IMS PCB layout composed of a

Manuscript received November 9, 2020; revised December 4, 2020; accepted December 11, 2020. Date of publication December 15, 2020; date of current version March 5, 2021. This work was supported in part by the Swiss Office of Energy under Grant SI/501887-01 (MEPCO) and in part by the European Research Council (ERC Starting Grant) under the European Union's H2020 Program/ERC Grant Agreement No. 679425. *(Corresponding authors: Armin Jafari; Elison Matioli.)*

The authors are with the Power and Wide-Band-Gap Electronics Research Laboratory, École Polytechnique Fédérale de Lausanne, Lausanne CH-1015, Switzerland (e-mail: armin.jafari@epfl.ch; mohammad.samizadeh@epfl.ch; remco.vanerp@epfl.ch; elison.matioli@epfl.ch).

Color versions of one or more figures in this letter are available at https://doi.org/10.1109/TPEL.2020.3045062.

Digital Object Identifier 10.1109/TPEL.2020.3045062

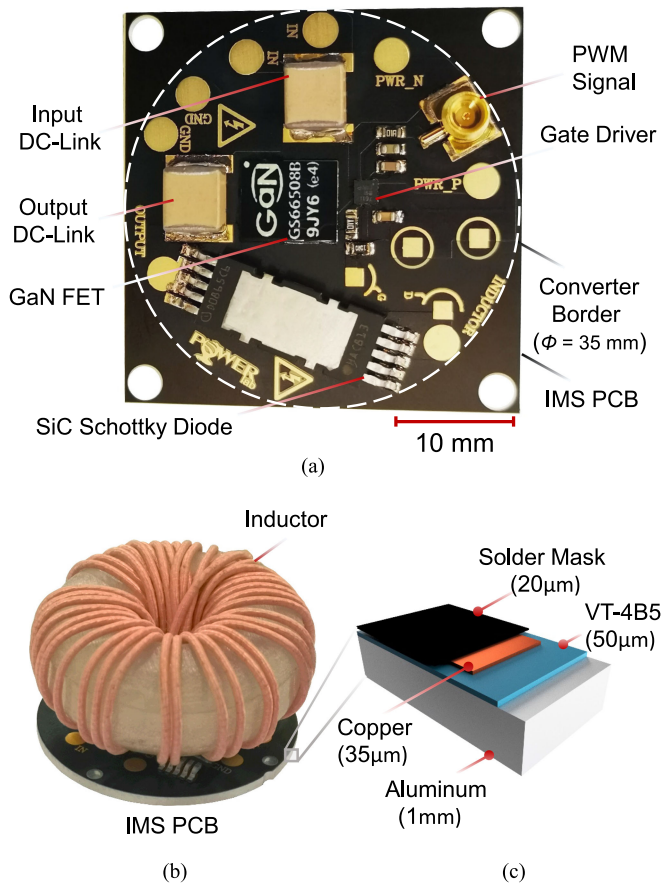

Fig. 1. Boost converter design using the IMS PCB technology. (a) Single-layer design of the power stage. (b) Compact final design with a 35-mm diameter. (c) PCB layout enables an extremely high thermal conductivity (>60 W/mK), suitable for the ultrahigh power density.

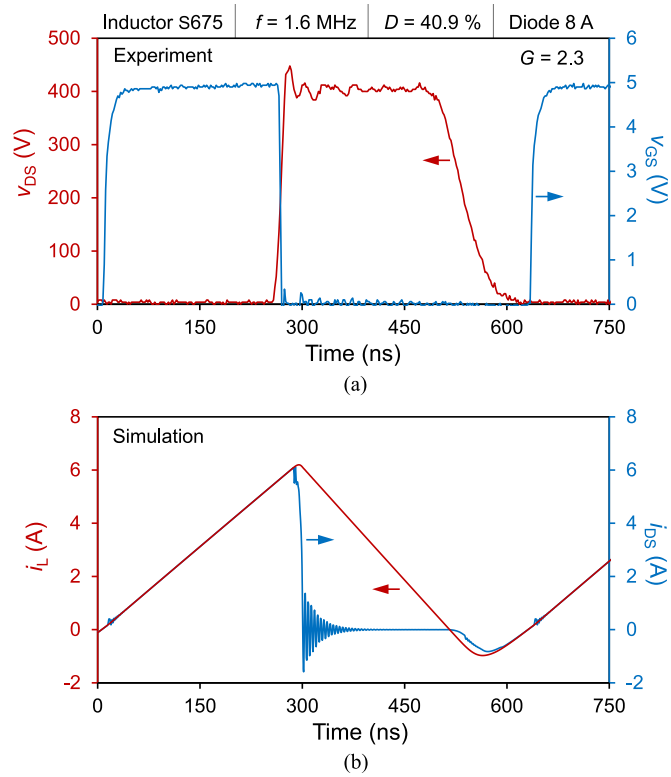

Fig. 2. Converter waveforms. (a) Experimental $v_{\rm DS}$ and $v_{\rm GS}$ waveforms measured with 1-GHz TPP1000 Tektronix voltage probes and with (b) i_L and $i_{\rm DS}$ waveforms extracted from spice simulation. The converter operated at 430 W of the input power and 400 V of the output voltage at $G = 2.3$. By adjusting the duty cycle, full ZVS is achieved, enabling high efficiencies at megahertz frequencies.

35-μm copper layer, a 50-μm VT4B5 insulation material, and a 1-mm aluminum substrate [see Fig. 1(c)]. The overall thermal conductivity k_t over the entire PCB thickness L_t can be expressed as

$$k_t = \frac{L_t}{L_1/k_1 + L_2/k_2 + L_3/k_3} \tag{1}$$

in which $k_1 = 385$ W/mK, $k_2 = 4.2$ W/mK, and $k_3 = 205$ W/mK represent the thermal conductivities of copper, VT4B5 insulation material, and aluminum, respectively, and L_1–L_3 are the corresponding thicknesses of each layer. Using (1), the IMS PCB offers $k_t > 60$ W/mK. Considering the board cross-sectional area, an overall thermal resistance of < 0.02 K/W was obtained, which is much lower than the junction-to-case thermal resistance of the transistor (0.5 K/W for GS66508B) and the diode ($\sim$1 K/W for IDDD08G65C6), granting a very efficient heat extraction from the devices. For better inductor cooling, one can employ high thermally conductive epoxies in the so-called *potting* process, which is widely used for improving the thermal performance of electrical machines, transformers, inductors, and transistor packages [7]–[10]. These materials fill the space between the windings and the IMS board and can provide up to two orders of magnitude higher thermal conductivities compared with air.

Additionally, the zero-voltage switching (ZVS) of the boost converter in the impulse rectification mode significantly reduced high-frequency losses [3]. To the same end, a GaN device (GS66508B) with very low soft-switching losses was selected [1]. Fig. 2(a) presents the gate-to-source ($v_{\rm GS}$) and drain-to-source ($v_{\rm DS}$) waveforms when the boost was fully soft switched at 1.6 MHz, with a 400-V dc output voltage and a voltage gain (G) of 2.3×. Inductor current i_L and drain-to-source current $i_{\rm DS}$ from spice simulation are shown in Fig. 2(b) for the same operating conditions.

III. Wide-Bandwidth Inductor Design

Power in a boost converter in the impulse rectification mode is regulated by switching frequency (f). To preserve a high efficiency over the entire load range, designing a wide-bandwidth inductor with high quality factor (Q) is essential. For an inductor with inductance L and ac resistance $R_{\rm AC}$, Q can be defined as

$$Q = 2\pi f L / R_{\rm AC} \tag{2}$$

which can be thought as the ratio of the energy stored in the inductor to the dissipated energy at each cycle. Therefore, improving Q directly results in higher efficiencies.

To optimize the inductor design, small-signal Q was measured for the spiral and toroidal inductors of comparable volumes, as listed in Table I. Using the same Litz wires (S675/AWG48),

TABLE I
COMPARISON OF INDUCTOR GEOMETRIES WITH CORE MATERIALS

Geometry	Core Material	Limitation
Spiral	Air	Magnetic field is not confined
Toroidal	Air	Maximum Q is limited
Toroidal	NiZn: 68	H_C is large, only good at low currents
Toroidal	MnZn: N49, N87	Q is not broad over frequency

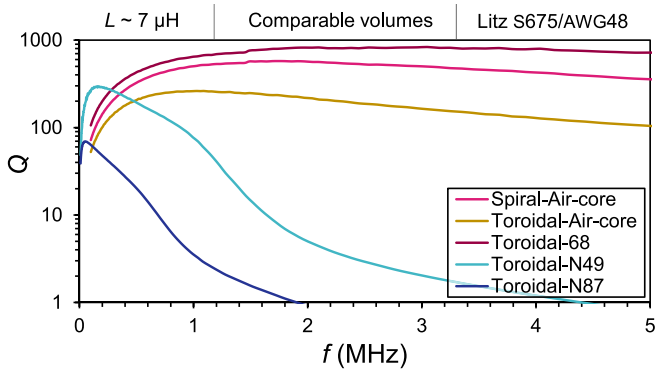

Fig. 3. Small-signal Q measurements for different inductor geometries and various high-frequency materials (as listed in Table I), using an E4990A keysight impedance analyzer. All the inductance values are close to 7 μH.

different materials were compared, as shown in Fig. 3. Although the ferrite 68 material exhibits the highest Q, due to a relatively large magnetic coercivity (H_C) of NiZn materials, the Q drops drastically at high currents [11], [12]. N49 and N87 MnZn ferrites operate efficiently (with $Q > 100$) only for a very limited frequency range. With the same overall size, air-core inductors present the widest bandwidths upon which $Q > 100$. Although the spiral inductor has a higher Q than its toroidal counterpart, its magnetic field is not confined and its Q is prone to substantial degradation in the vicinity of metallic objects (e.g., PCBs, cold plates, etc.). Therefore, we opted for the air-core toroidal design, as shown in Fig. 4(a).

In an air-core inductor with Litz windings, R_{AC} consists of a conductive resistance R_{COND} and a proximity-effect resistance R_{PROX}. R_{COND} is associated with the dc resistance and the skin effect over the strands, and R_{PROX} is the result of current crowding caused by external magnetic fields from adjacent conductors/strands [13]. Based on the theory proposed by Carretero *et al.* [14], R_{COND} is inversely proportional to the number of strands, whereas R_{PROX} scales linearly with the strand number. Additionally, R_{COND} affects Q in the low-frequency ranges, while R_{PROX} is dominant at high frequencies. Thus, for a fixed inductance value, one can change the strand number to tune the inductor Q and bandwidth. As Fig. 4(b) shows, by increasing the number of strands in the Litz winding from 180 to 1100, the peak of Q increases, while its bandwidth decreases.

In Fig. 4(c) and (d), the efficiency, η, versus input power (P_{IN}) and f is plotted for $G = 10$ and $G = 4$, respectively. The overall η has a strong dependence on the inductor Q. The inductor with 1100 strands (S1100) has the highest efficiency at $f < 0.5$ MHz [cf. Fig. 4(b) and (c)]. Nonetheless, for $f > 2$ MHz, the 180-strand design (S180) has the highest Q and, thus, the highest

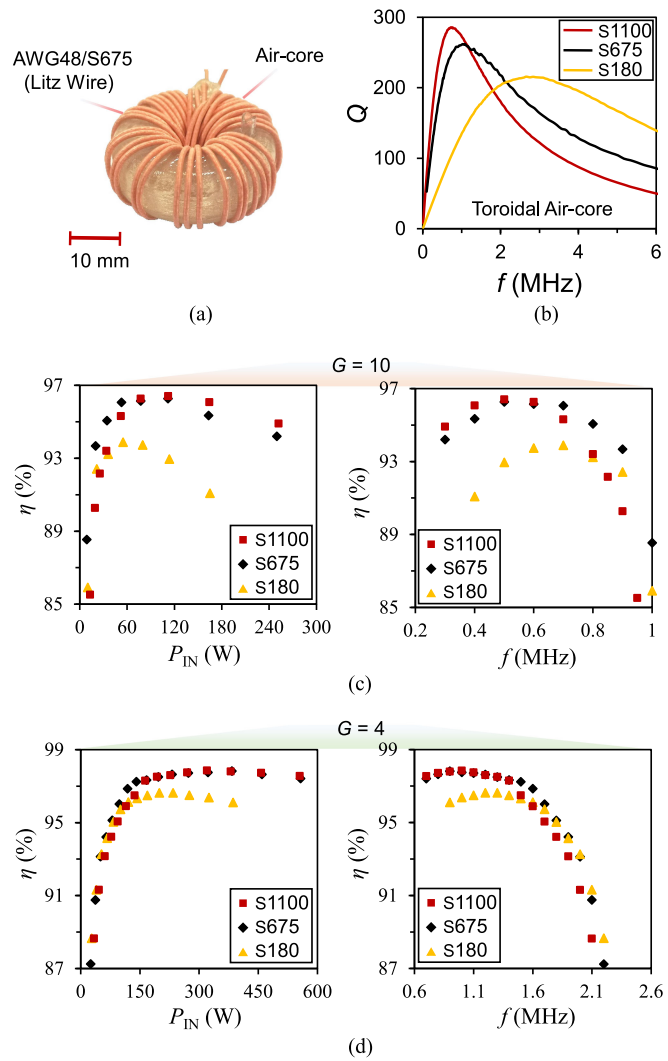

Fig. 4. Inductor design and its quality effect on the converter efficiency. (a) Toroidal inductor design with (b) small-signal Q measurements for various AWG48 Litz wires with strand numbers of 180, 675, and 1100. Boost efficiency versus the input power and frequency is presented for the voltage gains of (c) $G = 10$ and (d) $G = 4$. The small-signal Q of the inductor significantly affects the conversion efficiency, especially at higher voltage gains.

η [compare Fig. 4(b) and (d)]. The impact of inductor Q factor on η becomes more pronounced at higher G values [see Fig. 4(c) and (d)], whereas for low gains and high powers, the 675-strand design (S675) enables efficiencies similar to that of the 1100-strand design (S1100), as shown in Fig. 4(d), but at a lower cost. For optimizing other circuit parameters, the S675 inductor, which had the largest bandwidth below 3 MHz, was chosen.

IV. CHOICE OF THE DIODE

The zero reverse recovery in SiC Schottky diodes makes them great candidates for the high-frequency operation in the boost converter. Although synchronous rectification can potentially reduce the conduction losses, it increases layout design and control complexities. Thus, to optimize the efficiency with diode rectifiers, it is important to quantify the effect of device parameters on the overall η. Fig. 5(a) presents the junction capacitance

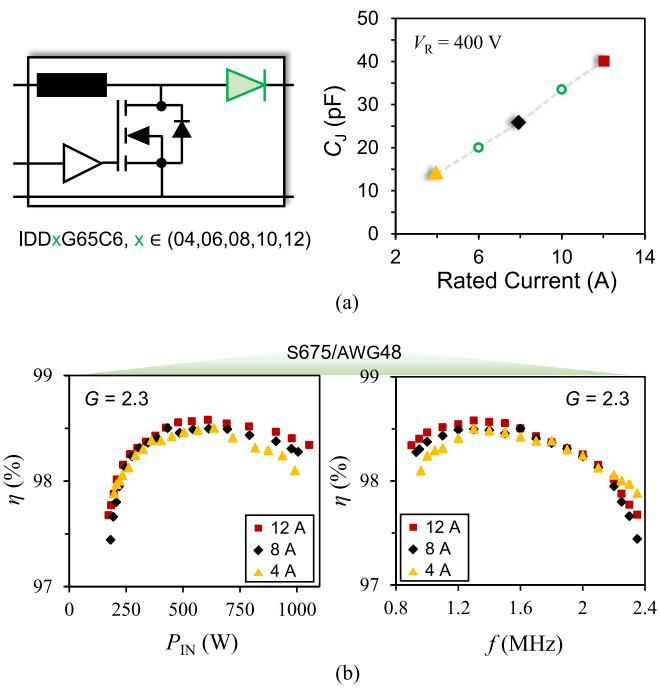

Fig. 5. (a) C_J versus the rated current for a family of SiC Schottky diodes. (b) η versus P_{IN} and f was extracted using 4-, 8-, and 12-A rated diodes. At light loads, the reactive power of C_J limits the efficiency, whereas at heavy loads, the conduction losses become dominant.

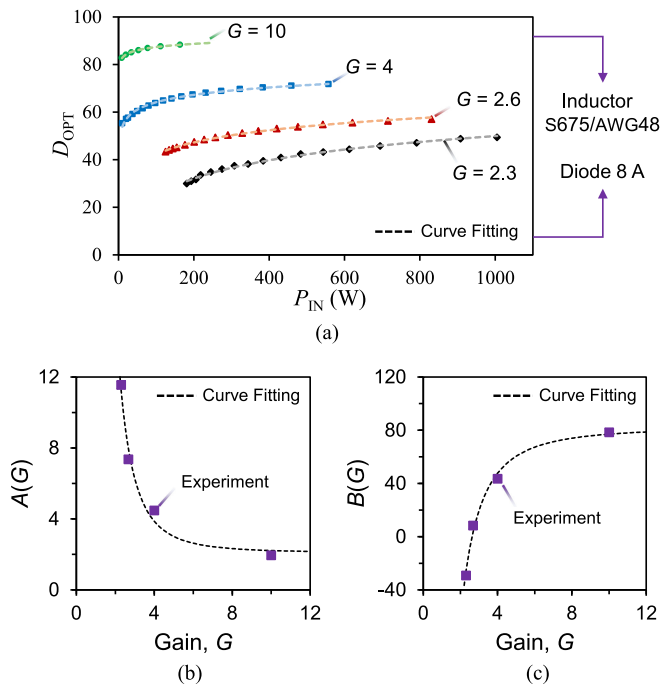

Fig. 6. Optimum duty cycle pattern. (a) D_{OPT} versus P_{IN}, showing its logarithmic dependence. (b) and (c) $A(G)$ and $B(G)$ versus G, used to determine D_{OPT} for a given voltage gain. The optimum duty cycle control is essential to the safe and efficient operation of boost converters in the impulse rectification mode.

C_J against the rated current for diodes with different current ratings (from a similar device family). C_J scales linearly with the current, increasing the reactive power, while at the same time, the device resistance and forward voltage drop decrease. For evaluating the effect of the aforementioned parameters on the converter efficiency, 4-A, 8-A, and 12-A diodes were operated up to 2.4 MHz and 1 kW, as shown in Fig. 5(b). The 12-A diode notably increased the efficiency at heavy loads, resulting in a peak efficiency of 98.6%. At high power levels, f is relatively low; thus, the conduction loss is dominant. Therefore, utilizing the diodes with higher rated currents improves the η. At light loads ($f > 2$ MHz), the diode with lower C_J (i.e., 4-A device) generates less reactive power, which in turn results in higher η. In all the cases, the air-core inductor (S675/AWG48) was employed.

V. Optimum Duty Cycle Control

Losing ZVS at high frequencies can result in a transistor failure due to excessive thermal and electrical stresses. In the impulse rectification regime, the power of a boost converter is regulated by f [3]; therefore, applying an optimum duty cycle D_{OPT} is essential to the safe and efficient operation of the converter. For $D > D_{OPT}$, the soft switching is compromised, and for $D < D_{OPT}$, less charging time is provided for the inductor, resulting in a low power transfer and reduced efficiencies, especially under light-load high-gain conditions [3].

Fig. 6(a) presents the D_{OPT} for the boost converter operating at various G values and different powers. D_{OPT} can be extracted as the function of the input power and voltage gain as

$$D_{OPT}(P_{IN}, G) = A(G)\ln(P_{IN}) + B(G). \tag{3}$$

At a fixed gain, D_{OPT} is a logarithmic function of P_{IN}. One can formulate coefficients $A(G)$ and $B(G)$ in (3) as

$$A(G) = c_0 + c_1 \Big/ \left(1 + \left(\frac{G}{c_2}\right)^{c_3}\right) \tag{4}$$

$$B(G) = d_0 + d_1 \Big/ \left(1 + \left(\frac{G}{d_2}\right)^{d_3}\right) \tag{5}$$

in which c_0–c_3 and d_0–d_3 are the constants extracted from the fitting of (4) and (5) to the experimental data, as shown in Fig. 6(b) and (c). By utilizing (3) in a real-time controller or deriving a lookup table and hard coding D_{OPT} values, the efficiency is maximized and the risk of device failure is eliminated.

VI. Benchmarking and Loss Breakdown

In Fig. 7(a), the boost converter is benchmarked against the state-of-the-art dc–dc converters in terms of peak efficiency and volumetric power density [4], [15]–[34]. The converter was operated at a fixed output voltage of 400 V and input voltages up to 175 V.

The efficiency of the converter (using the S675/AWG48 air-core inductor and the 12-A diode) at $G = 2.3$ reached a maximum of 98.6% (corresponding to $P_{IN} = 431.2$ W), and $\eta > 98\%$ was maintained up to $P_{IN} > 1$ kW. To identify the efficiency bottleneck, a comprehensive loss breakdown was performed using the device spice models and the measured transistor soft-switching losses [1]. The inductor was modeled by its parameters extracted from the small-signal Q measurements [see Fig. 4(b)]. Fig. 7(b)

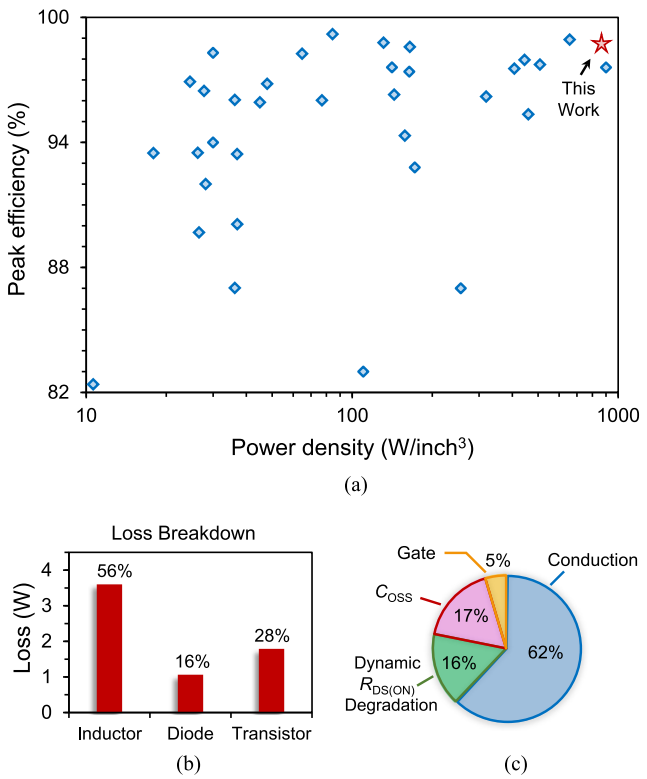

Fig. 7. (a) Peak efficiency versus volumetric power density for the state-of-the-art dc–dc converters [4], [15]–[34]. The red star indicates the demonstrated boost design in this letter. (b) System loss breakdown at $f = 1.6$ MHz and $P_{IN} = 431.2$ W with $\eta = 98.6\%$. The inductor is the efficiency bottleneck. (c) Transistor loss breakdown for GS66508B according to the measurement results from the article presented in [1].

presents a system-level loss breakdown at the most efficient operating point of the converter, and Fig. 7(c) summarizes the transistor losses due to its conduction and ON-resistance [$R_{DS(ON)}$] degradation as well as gate and output capacitance (C_{OSS}) losses [1], [35]. At $f = 1.6$ MHz and a peak current of 6 A, the inductor contributes to more than half of the overall converter losses. Despite its relatively high Q [$Q > 200$, see Fig. 4(b)], the inductor is still the bottleneck for obtaining higher efficiencies (and of course higher power densities). The development of new high-frequency magnetic materials is a key to higher efficiencies and power densities in converters based on inductive power transfer.

VII. Conclusion

A megahertz-class kilowatt-range boost converter based on the impulse rectification was optimized for high efficiency and high power density using high-performance GaN transistors and SiC Schottky diodes with a zero reverse recovery. A compact single-layer PCB design based on IMS technology enabled a superior thermal conductivity of > 60 W/mK. A comparison between different geometries and high-frequency materials resulted in designing wide-bandwidth toroidal air-core inductors. It was shown that the higher number of Litz wire strands in the air-core inductors increases the peak of quality factor and reduces the bandwidth, which can be adjusted to maximize the efficiency at different power levels. Using diodes with higher current ratings resulted in better efficiencies at high power levels; nonetheless, the major trade-off was the increased reactive power that degraded light-load efficiencies. We introduced an optimum duty cycle control strategy that maximizes the efficiency at any given operating point and prevents the risk of transistor failure due to an unwanted hard switching at extremely high frequencies. The boost converter was benchmarked against the state-of-the-art dc–dc converters, exhibiting an excellent figure of merit with a peak efficiency of 98.6% at an ultrahigh power density of 52 kW/l (850 W/in^3). Finally, a detailed loss breakdown identified the inductor losses as the efficiency bottleneck.

References

[1] A. Jafari *et al.*, "Comparison of wide-band-gap technologies for soft-switching losses at high frequencies," *IEEE Trans. Power Electron.*, vol. 35, no. 12, pp. 12595–12600, Dec. 2020.

[2] D. Neumayr, D. Bortis, and J. W. Kolar, "The essence of the little box challenge—Part A: Key design challenges & solutions," *CPSS Trans. Power Electron. Appl.*, vol. 5, no. 2, pp. 158–179, Jun. 2020.

[3] M. Samizadeh Nikoo, A. Jafari, N. Perera, and E. Matioli, "Efficient high step-up operation in boost converters based on impulse rectification," *IEEE Trans. Power Electron.*, vol. 35, no. 11, pp. 11287–11293, Nov. 2020.

[4] J. Biela, U. Badstuebner, and J. W. Kolar, "Impact of power density maximization on efficiency of DC–DC converter systems," *IEEE Trans. Power Electron.*, vol. 24, no. 1, pp. 288–300, Jan. 2009.

[5] E. Juntunen, A. Sitomaniemi, O. Tapaninen, R. Persons, M. Challingsworth, and V. Heikkinen, "Thermal performance comparison of thick-film insulated aluminum substrates with metal core PCBs for high-power LED modules," *IEEE Trans. Compon., Packag. Manuf. Technol.*, vol. 2, no. 12, pp. 1957–1964, Dec. 2012.

[6] F. Ludwig, T. Heidrich, and A. Mockel, "Integrated high-speed PMSM drive with IMS PCB-technology for mobile applications," in *Proc. IEEE 11th Int. Conf. Power Electron. Drive Syst.*, Jun. 2015, pp. 1070–1073.

[7] R. Kultzow, "High thermally conductive epoxy system for electrical and electronic thermal management," in *Proc. Elect. Insul. Conf. Elect. Manuf. Coil Winding Conf.*, 2001, pp. 285–289.

[8] S. Nategh, A. Boglietti, D. Barber, Y. Liu, and R. Brammer, "Thermal and manufacturing aspects of traction motors potting: A deep experimental evaluation," *IEEE Trans. Energy Convers.*, vol. 35, no. 2, pp. 1026–1035, Jun. 2020.

[9] U. Mehrotra *et al.*, "Packaging development for a 1200V SiC BiDFET switch using highly thermally conductive organic epoxy laminate," in *Proc. 32nd Int. Symp. Power Semicond. Devices ICs*, Sep. 2020, pp. 396–399.

[10] K. Fukushima, H. Takahashi, Y. Takezawa, M. Hattori, M. Itoh, and M. Yonekura, "High thermal conductive epoxy resins with controlled high-order structure," in *Proc. 17th Annu. Meeting IEEE Lasers Electro-Opt. Soc.*, 2004, pp. 340–343, doi: 10.1109/CEIDP.2004.1364257.

[11] R. S. Yang, A. J. Hanson, B. A. Reese, C. R. Sullivan, and D. J. Perreault, "A low-loss inductor structure and design guidelines for high-frequency applications," *IEEE Trans. Power Electron.*, vol. 34, no. 10, pp. 9993–10005, Oct. 2019.

[12] A. Jafari *et al.*, "Calibration-free calorimeter for sensitive loss measurements: Case of high-frequency inductors," in *Proc. IEEE 21st Workshop Control Model. Power Electron.*, Nov. 2020, pp. 1–8.

[13] Q. Deng *et al.*, "Frequency-dependent resistance of litz-wire square solenoid coils and quality factor optimization for wireless power transfer," *IEEE Trans. Ind. Electron.*, vol. 63, no. 5, pp. 2825–2837, May 2016.

[14] C. Carretero, J. Acero, and R. Alonso, "TM-TE decomposition of power losses in multi-stranded litz-wires used in electronic devices," *Prog. Electromagn. Res.*, vol. 123, pp. 83–103, 2012.

[15] L. Zhu, H. Bai, A. Brown, and M. McAmmond, "Two-stage vs one-stage design for a bidirectional 400V/12V 6kW auxiliary power module in electric vehicles," in *Proc. IEEE Transp. Electrific. Conf. Expo.*, Jun. 2020, pp. 1222–1226.

[16] L. Zhu, H. Bai, A. Brown, and M. McAmmond, "Design a 400V-12V 6kW bidirectional auxiliary power module for electric or autonomous vehicles with fast pre-charge dynamics and zero DC bias current," *IEEE Trans. Power Electron.*, to be published.

[17] G.-J. Su, C. White, and Z. Liang, "Design and evaluation of a 6.6 kW GaN converter for onboard charger applications," in *Proc. IEEE 18th Workshop Control Model. Power Electron.*, Jul. 2017, pp. 1–6.

[18] J. Scoltock, G. Calderon-Lopez, and A. J. Forsyth, "Topology and magnetics optimisation for a 100-kW bi-directional DC-DC converter," in *Proc. IEEE Veh. Power Propul. Conf.*, Dec. 2017, pp. 1–6.

[19] R. Ramachandran and M. Nymand, "Experimental demonstration of a 98.8% efficient isolated DC–DC GaN converter," *IEEE Trans. Ind. Electron.*, vol. 64, no. 11, pp. 9104–9113, Nov. 2017.

[20] J. Rabkowski, D. Peftitsis, and H.-P. Nee, "Parallel-operation of discrete SiC BJTs in a 6-kW/250-kHz DC/DC boost converter," *IEEE Trans. Power Electron.*, vol. 29, no. 5, pp. 2482–2491, May 2014.

[21] M. Pavlovsky, Y. Tsuruta, and A. Kawamura, "Pursuing high power-density and high efficiency in DC-DC converters for automotive application," in *Proc. IEEE Power Electron. Spec. Conf.*, Jun. 2008, pp. 4142–4148.

[22] M. Pavlovsky, Y. Tsuruta, and A. Kawamura, "Recent improvements of efficiency and power density of DC-DC converters for automotive applications," in *Proc. Int. Power Electron. Conf. ECCE Asia*, Jun. 2010, pp. 1866–1873.

[23] W. Liu, A. Yurek, B. Sheng, Y. Chen, Y.-F. Liu, and P. C. Sen, "A single stage 1.65kW AC-DC LLC converter with power factor correction (PFC) for on-board charger (OBC) application," in *Proc. IEEE Energy Convers. Congr. Expo.*, Oct. 2020, pp. 4594–4601.

[24] F. Krismer and J. W. Kolar, "Efficiency-optimized high-current dual active bridge converter for automotive applications," *IEEE Trans. Ind. Electron.*, vol. 59, no. 7, pp. 2745–2760, Jul. 2012.

[25] G. Kampitsis, R. van Erp, and E. Matioli, "Ultra-high power density magnetic-less DC/DC converter utilizing GaN transistors," in *Proc. IEEE Appl. Power Electron. Conf. Expo.*, Mar. 2019, pp. 1609–1615.

[26] D. Gunasekaran, "Switched capacitor-based DC-DC converter with ultra-high efficiency, power density and voltage regulation capability," Ph.D. dissertation, 2018.

[27] S. M. Fazeli, D. Jovcic, and M. Hajian, "Laboratory demonstration of closed-loop 30 kW, 200 V/900 v IGBT-based LCL DC/DC converter," *IEEE Trans. Power Del.*, vol. 33, no. 3, pp. 1247–1256, Jun. 2018.

[28] E. F. de Oliveira, S. Sprunck, J. Pfeiffer, and P. Zacharias, "A GaN-based DC/DC converter for E-vehicles applications," in *Proc. 22nd Eur. Conf. Power Electron. Appl.*, Sep. 2020, pp. P.1–P.10.

[29] P. Bazin, B. Beranger, J. Ecrabey, L. Garnier, and S. Mercier, "Smart fuel cell module (6.5 kW) for a range extender application," in *Proc. 22nd Eur. Conf. Power Electron. Appl.*, Lyon, France, Sep. 2020, pp. P.1–P.8.

[30] U. Badstuebner, J. Biela, D. Christen, and J. W. Kolar, "Optimization of a 5-kW telecom phase-shift DC–DC converter with magnetically integrated current doubler," *IEEE Trans. Ind. Electron.*, vol. 58, no. 10, pp. 4736–4745, Oct. 2011.

[31] A. Kawamura, M. Pavlovsky, and Y. Tsuruta, "State-of-the-art high power density and high efficiency DC-DC chopper circuits for HEV and FCEV applications," in *Proc. 13th Int. Power Electron. Motion Control Conf.*, Sep. 2008, pp. 7–20.

[32] B. Agrawal, L. Zhou, A. Emadi, and M. Preindl, "Variable-frequency critical soft-switching of wide-bandgap devices for efficient high-frequency nonisolated DC-DC converters," *IEEE Trans. Veh. Technol.*, vol. 69, no. 6, pp. 6094–6106, Jun. 2020.

[33] A. Jafari, M. Samizadeh Nikoo, F. Karakaya, N. Perera, and E. Matioli, "97.4%-efficient all-GaN dual-active-bridge converter with high step-up high-frequency matrix transformer," in *Proc. Int. Exhib. Conf. Power Electron., Intell. Motion, Renewable Energy Energy Manage.*, 2020, pp. 1–8.

[34] A. Jafari and E. Matioli, "High step-up high-frequency zero-voltage switched GaN-based single-stage isolated DC-DC converter for PV integration and future DC grids," in *Proc. Int. Exhib. Conf. Power Electron., Intell. Motion, Renewable Energy Energy Manage.*, 2018, pp. 1–6.

[35] M. Samizadeh Nikoo, A. Jafari, N. Perera, and E. Matioli, "Measurement of large-signal C_{OSS} and C_{OSS} losses of transistors based on nonlinear resonance," *IEEE Trans. Power Electron.*, vol. 35, no. 3, pp. 2242–2246, Mar. 2020.